Stability analysis on the free surface phenomena of a magnetic fluid for general use

Yo Mizuta[a,*]

[a]*Division of Applied Physics, Hokkaido University, Sapporo 060-8628, Japan*

Abstract

This paper presents an analysis for elucidating a variety of physical processes on the interface (free surface) of magnetic fluid. The present analysis is composed of the magnetic and the fluid analysis, both of which have no limitations concerning the interface elevation or its profile. The magnetic analysis provides rigorous interface magnetic field under arbitrary distributions of applied magnetic field. For the fluid analysis, the equation for interface motion includes all nonlinear effects. Physical quantities such as the interface magnetic field or the interface stresses, obtained first as the wavenumber components, facilitate confirming the relations with those by the conventional theoretical analyses. The nonlinear effect is formulated as the nonlinear mode coupling between the interface profile and the applied magnetic field. The stability of the horizontal interface profile is investigated by the dispersion relation, and summarized as the branch line. Furthermore, the balance among the spectral components of the interface stresses are shown, within the sufficient range of the wavenumber space.

PACS: 41.20.Gz; 47.11.-j; 47.20.-k; 47.20.Ky; 47.35.-i; 47.35.Tv; 47.54.-r; 47.65.-d; 47.65.Cb; 52.35.Mw

Keywords: Magnetic fluid, Magnetic field, Free surface, Instability, Bifurcation, Numerical analysis

*Corresponding author. Tel.: +81-11-706-6708; fax: +81-11-706-6859.
Email address: yomizuta@eng.hokudai.ac.jp (Yo Mizuta)

1. Introduction

Free surface phenomena of magnetic fluid, especially the transition among the patterns of flat, hexagonal and square on the horizontal interface profile, have been of major interest in magnetic fluid science. Just after the magnetic fluid was invented, many experiments were conducted together with basic analyses [1, 2] preceding nonlinear analyses.

Though the onset of the transition can be found by these linear analysis, the pattern formation phenomena is essentially nonlinear, as analyzed by Gailitis [3], or Twombly-Thomas [4, 5]. However, the nonlinear analysis then usually adopts the perturbation method, that is, quantities on the interface are expanded into finite power series of the interface elevation; In addition, the applied magnetic field is limited to vertical and homogeneous, which usually differs from the conditions in experiments.

Afterward, high performance computers and the development in the numerical techniques to treat continuous media enabled numerical simulation [6]. The conventional approach has been the FEM by use of the irregular fine lattices dividing the real space.

As the intensity of the magnetic field applied on the interface of magnetic fluid is increased, transitions are caused when the balance among the interface stresses is changed. These phenomena are necessarily analyzed by using rigorous interface magnetic fields even on arbitrarily deformed interfaces under arbitrarily applied magnetic fields. In [7], we showed a method to determine the spectral components of the interface magnetic fields rigorously from a set of "three-dimensional interface magnetic field equations" with the help of the property of the "three-dimensional Hilbert transform" on periodic functions. For some different interface profiles, distributions of the interface magnetic fields and the interface stresses were calculated.

In the conventional numerical stability analysis, the bifurcation diagram seems to be produced from the appearance of the interface profiles in the real space [6]. Instead, the present research follows the approach adopted by the existing theories, and tries to compare their results. That is, we obtain the quantities on the interface as the spectral components first. Then, we draw a branch line according to its definition, as shown in this paper. Actually, the interface magnetic fields were found to be obtained more compactly than as in [7], which is shown in Section 2. The magnetic fields thus obtained are used for the interface magnetic stress difference. It determines the behaviour of the interface through the balance with other interface stresses. This is in-

vestigated by the "equation for interface motion"that includes all nonlinear effects (Section 3.1). The interaction between the applied magnetic field and the interface profile is formulated as the nonlinear mode coupling. The stability of the interface is discussed by the dispersion relation, and summarized as the branch line (Section 3.4). Section 4 presents those results for the interface profile of two-dimensional and a hexagonal lattice. Furthermore, the balance among the spectral components of the interface stresses are shown at the critical intensity of the applied magnetic field, within the sufficient range of the wavenumber space.

2. Interface magnetic field analysis

The magnetic stress difference

$$T \equiv -\,[1/\,\mu_j]\{\mu_1\mu_2(h_X^2 + h_Y^2) + b_Z^2\}/\,2 \tag{1}$$

represents the action from the magnetic field to the fluid, where μ_j denotes the permeability of the fluid (j=1) or the vacuum (j=2), $[\cdots]$ the difference of the value across the interface (2−1), and $h_{X,Y}$, b_Z are the tangential magnetic field and the normal magnetic flux, respectively. These interface magnetic fields should be obtained rigorously as well as efficiently under arbitrary interface profiles and arbitrarily applied magnetic field distributions.

Each of the interface magnetic fields is divided into the **basic field** $h_{X,Y}^0$, b_Z^0 and the **induced field** $h_{X,Y}^1$, b_Z^1. Basic fields are given directly by a known applied magnetic field $\boldsymbol{h}^0$ as $h_{X,Y}^0 = \boldsymbol{t}_{X,Y}\cdot\boldsymbol{h}^0$ and $b_Z^0 = \boldsymbol{t}_Z\cdot\boldsymbol{h}^0/\,P$ where $\boldsymbol{t}_{X,Y}$ are the tangential unit vectors, $\boldsymbol{t}_Z$ is the normal unit vector, and $P \equiv (1/\,\mu_2 + 1/\,\mu_1)/\,2$. Induced fields are to be determined to satisfy, together with the basic fields, both the harmonic property and the interface conditions, as discussed in [7]. Instead of solving the set of **three-dimensional interface magnetic field equations**, however, induced fields are obtained equivalently but simply as

$$\begin{cases} h_X^1 = \hat{G}_X\,(1 + M\hat{G}_Z)^{-1}\tilde{h}_Z, \\ h_Y^1 = \hat{G}_Y\,(1 + M\hat{G}_Z)^{-1}\tilde{h}_Z, \\ b_Z^1 = \hat{G}_Z\,(1 + M\hat{G}_Z)^{-1}\tilde{h}_Z, \end{cases} \tag{2}$$

where $\tilde{h}_Z = -\,M_{\rm n}/\,2$ is the source term for the induced fields, $M_{\rm n} = 2Mb_Z^0$ is the normal magnetization, and $M \equiv (1/\,\mu_2 - 1/\,\mu_1)/\,2$.

The **three-dimensional Hilbert transform operators** $\hat{G}_I$ (I=X,Y,Z) are defined as follows:

$$\begin{aligned} \hat{G}_{X,Y}\{g(\boldsymbol{R}')\} &= \hat{H}\left\{\boldsymbol{t}_{X,Y}\cdot\nabla' g(\boldsymbol{R}')\right\}, \\ \hat{G}_Z\{g(\boldsymbol{R}')\} &= \frac{1}{P}\hat{H}\left\{\boldsymbol{t}_Z\cdot\nabla' g(\boldsymbol{R}')\right\}, \\ \hat{H}\left\{g(\boldsymbol{R}')\right\} &\equiv -2\iint \mathrm{d}S'\psi g(\boldsymbol{R}'), \end{aligned} \tag{3}$$

where $g(\boldsymbol{R}')$ is an arbitrary function of the interface coordinate parameter $\boldsymbol{R}'$=(X', Y'). The position vectors for the observation point and the source point are denoted by $\boldsymbol{r}$=$\boldsymbol{r}(\boldsymbol{R})$ and $\boldsymbol{r}'$=$\boldsymbol{r}(\boldsymbol{R}')$. The functions and the derivatives for the source point are shown by "$'$". The operator $\hat{H}$ is composed of the integral over the source point on the interface and the basic solution of the three-dimensional Poisson equation as

$$\psi = -\frac{1}{4\pi|\boldsymbol{r}'-\boldsymbol{r}|}, \quad \nabla'\psi = \frac{\boldsymbol{r}'-\boldsymbol{r}}{4\pi|\boldsymbol{r}'-\boldsymbol{r}|^3}. \tag{4}$$

The operation of $\hat{G}_I$ is evaluated analytically instead of by the numerical integration if its operand is expanded into a series of periodic functions. These operations result in just the derivatives with respect to X' or Y', or the nonlinear mode coupling between the interface profile and the applied magnetic field (Appendix A).

3. Stability analysis

3.1. Equation for interface motion

When we analyze the free surface phenomena of irrotational and invscid magnetic fluid without the temperature dependence of the magnetization, we use the following **equation for interface motion** which is derived from Bernoulli's equation and the dynamic boundary condition on the interface:

$$\rho\frac{\partial\varphi}{\partial t} + S + p_0 = 0, \quad S \equiv D + G + C + T, \tag{5}$$

where ρ, φ, D, G, C, T, p_0 are the fluid density, velocity potential, dynamic pressure, gravity potential, surface tension, magnetic stress difference of (1), and atmospheric pressure, respectively.

The velocity potential φ and the sum of stresses S depend on the interface elevation z^1. When they are linearized for infinitesimal $z^1 \propto \exp\{\mathrm{i}(\omega t - \boldsymbol{k}\cdot\boldsymbol{r})\}$,

the following dispersion relation for linear wave motion is derived from (5) [8]:

$$\omega^2 = gk + (\gamma/\rho)\, k^3 - \left(M_{\rm n}^2/\, 2\rho P\right) k^2, \tag{6}$$

where g, γ, ω, k are the gravity acceleration, capillary coefficient, angular frequency, and amplitude of the wavenumber vector $\boldsymbol{k}$, respectively. In the linear harmonic analysis, we use b_Z^0 and $M_{\rm n}$ where $\boldsymbol{t}_Z{\cdot}\boldsymbol{h}^0$ is replaced with the applied magnetic field intensity H_0. Further, the induced field of the normal magnetic flux is $b_Z^1 = M_{\rm n} k z^1/\, 2P$, in proportion to z^1 (Appendix B).

As H_0 is increased, the transition from a stable state with a flat interface to an unstable state occurs. The critical wavenumber $k_{\rm CL}$ and the critical magnetic field intensity $H_{\rm CL}$ are:

$$\begin{cases} k_{\rm CL} \equiv (\rho g/\, \gamma)^{1/2}, \\ H_{\rm CL} \equiv P M_{\rm CL}/\, 2M, \quad M_{\rm CL}^2 \equiv 4P\, (\rho g \gamma)^{1/2} \end{cases} \tag{7}$$

from the condition that ω satisfying the dispersion relation (6) first has the imaginary part, or $\omega^2 = 0$ and $\partial\omega^2/\partial k = 0$ [8].

3.2. Expansion into series of periodic functions

We expand here the interface elevation $z^1(\boldsymbol{R})$ and the sum of interface stresses $S(\boldsymbol{R})$ into series of periodic functions as:

$$z^1(\boldsymbol{R}) = \boldsymbol{\Phi}^{(zS)}(\boldsymbol{R})\tilde{\boldsymbol{z}}^1, \quad S(\boldsymbol{R}) = \boldsymbol{\Phi}^{(zS)}(\boldsymbol{R})\tilde{\boldsymbol{S}}, \tag{8}$$

where

$$\begin{aligned} \boldsymbol{\Phi}^{(zS)}(\boldsymbol{R}) &= \left(\begin{array}{c|c} {\scriptstyle 1\cdots\mu\cdots N_S} & {\scriptstyle 1\cdots\mu\cdots N_A} \\ \cos\Theta_\mu & \sin\Theta_\mu \end{array}\right) \\ &= \left(\begin{array}{c|c} {\scriptstyle 1\cdots\mu\cdots N_S} & {\scriptstyle 1\cdots\mu\cdots N_A} \\ f_\mu^S(\boldsymbol{R}) & f_\mu^A(\boldsymbol{R}) \end{array}\right) \equiv \left(\begin{array}{c} {\scriptstyle 1\cdots\mu\cdots N} \\ f_\mu(\boldsymbol{R}) \end{array}\right) \end{aligned} \tag{9}$$

is the row vector of periodic functions with $N{=}N_S{+}N_A$ components, $\tilde{\boldsymbol{z}}^1 \equiv \left(\tilde{z}_\mu^1\right)$ and $\tilde{\boldsymbol{S}} \equiv \left(\tilde{S}_\mu\right)$ are the column vectors of expansion coefficients, and $\Theta_\mu \equiv \boldsymbol{k}_\mu{\cdot}\boldsymbol{R}$ is defined with the wavenumber vector $\boldsymbol{k}_\mu$.

The velocity potential in (5) is obtained from the vertical component of the fluid velocity v_z as $\varphi = \int_{-\infty}^{z^1} {\rm d}z v_z$, where k-th component of v_z is $(\partial z^1/\partial t)\, {\rm e}^{kz}$. Then, the equation for interface motion (5) reduces to the equation for $\tilde{\boldsymbol{z}}^1$ as

$$\begin{aligned} &\partial^2\tilde{\boldsymbol{z}}^1/\partial t^2 = -\, k\tilde{\boldsymbol{S}}(\tilde{\boldsymbol{z}}^1)\Big/\rho, \\ &\tilde{\boldsymbol{S}}(\tilde{\boldsymbol{z}}^1) = \tilde{\boldsymbol{G}}(\tilde{\boldsymbol{z}}^1) + \tilde{\boldsymbol{C}}(\tilde{\boldsymbol{z}}^1) + \tilde{\boldsymbol{T}}(\tilde{\boldsymbol{h}}_X(\tilde{\boldsymbol{z}}^1), \tilde{\boldsymbol{h}}_Y(\tilde{\boldsymbol{z}}^1), \tilde{\boldsymbol{b}}_Z(\tilde{\boldsymbol{z}}^1)), \end{aligned} \tag{10}$$

where $\tilde{\boldsymbol{G}}$, $\tilde{\boldsymbol{C}}$ and $\tilde{\boldsymbol{T}}$ are column vectors of the expansion coefficients for G, C and T, respectively.

3.3. Relation between expansion coefficients

The functional relation $\tilde{\boldsymbol{S}}(\tilde{\boldsymbol{z}}^1)$ must be established exactly for practical analyses, though just symbolically shown in this paper. Since G and C depend on the interface profile directly, the relations $\tilde{\boldsymbol{G}}(\tilde{\boldsymbol{z}}^1)$ and $\tilde{\boldsymbol{C}}(\tilde{\boldsymbol{z}}^1)$ are rather straightforward. In contrast, $\tilde{\boldsymbol{T}}$ depends on $\tilde{\boldsymbol{z}}^1$ in a complex manner through the expansion coefficients of interface magnetic fields $\tilde{\boldsymbol{h}}_{X,Y}$ and $\tilde{\boldsymbol{b}}_Z$, since T is a function of the interface magnetic fields practically.

Once the relation $\tilde{\boldsymbol{S}}(\tilde{\boldsymbol{z}}^1)$ is established, we can obtain the gradient matrix

$$\mathsf{H} \equiv \left(\frac{\partial \tilde{\boldsymbol{S}}}{\partial \tilde{z}^1_\mu} \right)^{1 \cdots \mu \cdots N}. \tag{11}$$

This matrix is used for several purposes: The accuracy of computing the interface stresses is checked by comparing H obtained theoretically and numerically; The inverse matrix of H is used when Newton's method is applied for determining the stationary interface profile; The critical magnetic field intensity H_c is found for finite interface elevations instead of (7), as discussed in the next subsection.

3.4. Determination of critical magnetic field intensity

Equation (10) shows that $h_\mu \equiv k\tilde{S}_\mu \Big/ \rho \tilde{z}^1_\mu$ corresponds to the right hand side of the dispersion relation (6), where h_μ represents the response of the sum of interface stresses at the same wavenumber as given to the interface profile. By the correspondence between the right hand side of (6) and $k\mathsf{H}/\rho$ from (10) and (11), this consideration is generalized for finite interface elevations with multimode. **The transition of stability arises when the smallest eigenvalue h of H first crosses zero as the intensity of the applied magnetic field H_0 increases.**

At each ζ_0, the typical value of the amplitude of z^1, we determine $H_0{=}H_\mathrm{c}$ to satisfy $h = 0$, and plot a point on the (H_0, ζ_0) plane. By connecting these points, we can draw a **branch line**, in the right of which an unstable state occurs.

Figure 1

Figure 2

Figure 3

4. Comparison of theoretical and numerical results

In this section, we present some properties on the free surface phenomena of magnetic fluid for the interface profile of two-dimensional and a hexagonal lattice.

We consider here a magnetic fluid with the fluid density ρ=1.0 $\times 10^3$ [kg m^{-3}], the capillary coefficient γ=2.6 $\times 10^{-2}$ [N m^{-1}], and the magnetic permeability $\mu_1/\,\mu_0$=1.40 ($\mu_2/\,\mu_0$=1.00, μ_0=4π $\times 10^{-7}$ [H/m]). Then, the critical wavenumber is $k_{\rm CL}$=6.14 $\times 10^2$ [m^{-1}] (critical wavelength is $\lambda_{\rm CL}$=1.02 $\times 10^{-2}$ [m]), and the critical magnetic field intensity is $H_{\rm CL}$=1.98 $\times 10^4$ [A/m] (magnetic pressure is 9.77 $\times 10^{-3}$ [mH_2O]), as obtained from (7) for the linearized case.

4.1. Case of two-dimensional interface profile

We choose the horizontal length of the spatial region h_0=5.0 $\times 10^{-2}$ [m] so that h_0 is some times of the critical wavelength $\lambda_{\rm CL}$. We give the horizontal interface profile by a unique mode with the wavenumber k=mk_0 (k_0= $\pi/\,h_0$: basic wavenumber, m: even number, $0 \le m \le M$=36) and the amplitude ζ_0 between 0.2 $\times 10^{-4}$ [m] and 5.0 $\times 10^{-4}$ [m]. For the calculation of the surface tension, for example, the spatial region is divided into N=40 subsections. Since their interval Δx= $h_0/\,N$ must be less than the half of the minimum wavelength $\lambda_{\rm min}$= $2h_0/\,M$, we choose M and N as $M<N$.

Figure 4

Figure 5

Under a vertical and homogeneous magnetic field with the intensity of H_0=$H_{\rm CL}$, we compare the response h_μ and the interface magnetic flux b_Z^1 with those by the linear harmonic analysis in Fig. 1 (a). For smaller ζ_0 of (1), dots of the numerical results lie well on lines of the linear harmonic analysis. However, in (2), dots shift toward positive than lines.

Figure 1 (b) shows the spectral distribution of the interface magnetic field. The components other than the component k_μ (close to $k_{\rm CL}$) given originally to the interface profile are generated more for (2) due to the nonlinear mode coupling between the interface profile and the magnetic field. As a result, both the interface magnetic field and the magnetic stress difference at k_μ decrease, and h_μ shifts toward positive.

Figure 2 (a) shows the dependence of the smallest eigenvalue h of H on the intensity of the applied magnetic field H_0. Since h is larger for larger ζ_0, the critical magnetic field $H_{\rm c}$ is larger, too. Figure 2 (b) shows a **supercritical branch line**, drawn as explained in Section 3.4.

4.2. Case of hexagonal-lattice interface profile

An interface profile of a hexagonal lattice as shown in Fig. 3 (a) is generated by

$$z^1(\boldsymbol{R}) = \sum_{\mu=0}^{3} \tilde{z}^1_{S\mu} \cos \boldsymbol{k}_\mu \cdot \boldsymbol{R} \tag{12}$$

of (8) with

$$\begin{cases} \boldsymbol{k}_0 = 0\boldsymbol{A} + 0\boldsymbol{B}, & \tilde{z}^1_{S0} = 0, \\ \boldsymbol{k}_1 = 2\boldsymbol{A} + 0\boldsymbol{B}, & \tilde{z}^1_{S1} = \zeta_0, \\ \boldsymbol{k}_2 = 0\boldsymbol{A} + 2\boldsymbol{B}, & \tilde{z}^1_{S2} = \zeta_0, \\ \boldsymbol{k}_3 = 2\boldsymbol{A} + 2\boldsymbol{B}, & \tilde{z}^1_{S3} = \zeta_0, \end{cases}$$

where $\boldsymbol{A} = (\hat{X} - \sqrt{3}\hat{Y})\pi \Big/ (2\sqrt{3}h_0)$, $\boldsymbol{B} = (\hat{X} + \sqrt{3}\hat{Y})\pi \Big/ (2\sqrt{3}h_0)$ are reciprocal lattice vectors, ζ_0, h_0 are vertical and horizontal scaling factors, and $\hat{X}$, $\hat{Y}$ are unit vectors orthogonal to each other. Three modes with nonzero spectral components of z^1 are shown by circles in the wavenumber space of Fig. 3 (b). The dispersion relation (6) was originally derived for the two-dimensional interface profile. However, it is considered from (A.4) that we are allowed to use (6) even for the three-dimensional case, when the amplitudes of all the wavenumber vectors composing z^1 are equal to k, as in the present case. Shaded squares in Fig. 3 (b) show the value of ω^2 of (6) at each wavenumber when $H_0 = H_{\mathrm{CL}}$, and the curve represents the position of the critical wavenumber k_{CL}.

Figure 3 (c) shows the branch line in the (H_0, ζ_0) plane under a vertical and homogeneous magnetic field. Such a **subcritical branch line** predicts to cause the hysteresis [3, 6].

During this analysis, it has been concerned whether the wavenumber range $\boldsymbol{k}_\mu = m_1\boldsymbol{A} + m_2\boldsymbol{B}$ (m_1, m_2: even numbers, $0 \leq m_1, m_2 \leq M = 18$) is wide enough, or not, to cover the spread of modes due to the nonlinear mode coupling. Figure 4 shows the wavenumber spectra of the interface stresses just when S reaches around zero at most wavenumbers after the balance among T, C and G. Three typical modes in T and C are reduced in S, which shows the balance among the stresses. However, we observe the spread in the spectral distribution of S. Figure 5 shows the average and the standard deviation σ of the spectra of the stresses at $H_0 = H_{\mathrm{c}}$ for each ζ_0, which are weighted by the spectral intensity, and normalized to the total wavenumber range. From these, the prepared wavenumber range seems to

cover the spread in the spectral distribution, where T depends on ζ_0 most sensitively other than S.

5. Conclusions

Stability analyses for the transition of patterns on the interface of magnetic fluid are performed. Both of the magnetic and the fluid analysis used do not employ the perturbation approach; Instead, the spectral components of the quantities on the interface are obtained first, which facilitates the comparison with the results by the conventional linear and weakly nonlinear analyses. Interface magnetic fields can be obtained rigorously on arbitrary interface profiles under arbitrarily applied magnetic field distributions. The fluid is analyzed by the equation for interface motion with all nonlinear effects.

The stability of the interface is discussed by the dispersion relation, which is extended from the infinitesimal interface elevation to the finite interface elevation by the gradient matrix. The critical intensity of the applied magnetic field is determined from the eigenvalue of the gradient matrix which decreases with the increase of the intensity of the applied magnetic field.

The calculated results for the interface profile of two-dimensional and a hexagonal lattice are presented. The branch line for the hexagonal-lattice case is subcritical though that for the two-dimensional case is supercritical. Transitions are caused when the balance among the interface stresses is changed as the intensity of the magnetic field applied on the interface of magnetic fluid is increased. This is actually shown by the spectra of the interface stresses within the sufficient range of the wavenumber space.

The range of ζ_0, the typical value of the amplitude of z^1, is still to be enlarged. For exploring this range, the stability of the system is observed carefully by changing the set (H_0, ζ_0). Instead, for more efficiency, the horizontal scaling factor h_0 is adjusted to tune up the critical wavenumber k_c. This process should be automated though done manually at present.

Appendix A. Operation of three-dimensional Hilbert transform operators

From the definition in (3), the three-dimensional Hilbert transform operators $\hat{G}_I$ are written as

$$\begin{aligned}\hat{G}_{X,Y}\{g(\boldsymbol{R}')\} &\equiv 2\iint \mathrm{d}S'(\boldsymbol{t}_{X,Y}\cdot\nabla'\psi)g(\boldsymbol{R}'),\\ \hat{G}_Z\{g(\boldsymbol{R}')\} &\equiv \frac{2}{P}\iint \mathrm{d}S'(\boldsymbol{t}_Z\cdot\nabla'\psi)g(\boldsymbol{R}').\end{aligned} \tag{A.1}$$

We compose an orthogonal curvilinear coordinate by $\boldsymbol{t}_{X,Y,Z}$ at $\boldsymbol{R}$, and express $\boldsymbol{r}'-\boldsymbol{r}$, by using the tangential coordinate vector $\boldsymbol{\rho}'$, as

$$\begin{aligned}\boldsymbol{r}'-\boldsymbol{r} &= \boldsymbol{\rho}'+\zeta(\boldsymbol{R}')\boldsymbol{t}_Z(\boldsymbol{R}),\\ \boldsymbol{\rho}' &= \xi(\boldsymbol{R}')\boldsymbol{t}_X(\boldsymbol{R})+\eta(\boldsymbol{R}')\boldsymbol{t}_Y(\boldsymbol{R}).\end{aligned}$$

In the denominator of $\nabla'\psi$, $|\boldsymbol{r}'-\boldsymbol{r}|$ is approximated by $\rho'=|\boldsymbol{\rho}'|$, and the interface profile function $\zeta(\boldsymbol{R}')\equiv\boldsymbol{t}_Z\cdot(\boldsymbol{r}'-\boldsymbol{r})$ is defined and used in its numerator. Furthermore, the relation

$$\frac{1}{(\rho')^3} = -\left(\boldsymbol{t}_X\frac{\partial}{\partial\xi'}+\boldsymbol{t}_Y\frac{\partial}{\partial\eta'}\right)\cdot\frac{\boldsymbol{\rho}'}{(\rho')^3}$$

is used, and each equation in (A.1) is integrated by parts. Then, (A.1) is rewritten as

$$\begin{aligned}\hat{G}_{X,Y}\{g(\boldsymbol{R}')\} &= \iint \mathrm{d}S'\frac{\boldsymbol{t}_{X,Y}\cdot\boldsymbol{\rho}'}{2\pi|\boldsymbol{r}'-\boldsymbol{r}|^3}g(\boldsymbol{R}')\\ &\simeq \hat{H}^*\left\{\frac{\partial g(\boldsymbol{R}')}{\partial\xi'}\right\},\ \hat{H}^*\left\{\frac{\partial g(\boldsymbol{R}')}{\partial\eta'}\right\},\\ \hat{G}_Z\{g(\boldsymbol{R}')\} &= \frac{1}{P}\iint \mathrm{d}S'\frac{1}{2\pi|\boldsymbol{r}'-\boldsymbol{r}|^3}\zeta(\boldsymbol{R}')g(\boldsymbol{R}')\\ &\simeq \hat{H}^*\left\{\left(\frac{\partial^2}{\partial(\xi')^2}+\frac{\partial^2}{\partial(\eta')^2}\right)\zeta(\boldsymbol{R}')g(\boldsymbol{R}')\right\},\\ \hat{H}^*\{g(\boldsymbol{R}')\} &\equiv \iint \mathrm{d}\xi'\mathrm{d}\eta'\frac{1}{2\pi\rho'}g(\boldsymbol{R}').\end{aligned} \tag{A.2}$$

We expand here the interface profile function and the operand function (magnetic field) into series of periodic functions like $f_\nu(\boldsymbol{R})=\cos\Theta_\nu,\sin\Theta_\nu$ $(\Theta_\nu\equiv k_{\nu X}X+k_{\nu Y}Y)$, as follows:

$$\zeta(\boldsymbol{R}')=\sum_{\mu=0}^{\infty}\tilde{\zeta}_\mu f_\mu(\boldsymbol{R}'),\quad g(\boldsymbol{R}')=\sum_{\nu=0}^{\infty}\tilde{g}_\nu f_\nu(\boldsymbol{R}').$$

Hereafter, the operation of $\hat{G}_I$ concerns on the periodic function. In [7],

$$\hat{H}^*\{f_\nu(\boldsymbol{R}')\} = f_\nu/\,k_\nu \tag{A.3}$$

was shown, where $x_\nu \equiv k_{\nu X}/\left|\boldsymbol{r}_X\right|$, $y_\nu \equiv k_{\nu Y}/\left|\boldsymbol{r}_Y\right|$, $k_\nu^2 \equiv x_\nu^2 + y_\nu^2$ are the components and the amplitude of the effective wavenumber, with $\left|\boldsymbol{r}_X\right| \equiv \left|\partial \boldsymbol{r}/\partial X\right|$, $\left|\boldsymbol{r}_Y\right| \equiv \left|\partial \boldsymbol{r}/\partial Y\right|$ which appear at the transformation of variables $\xi' = \left|\boldsymbol{r}_X\right|(X' - X)$ and $\eta' = \left|\boldsymbol{r}_Y\right|(Y' - Y)$. When the periodic functions are trigonometric functions, their product is written as $f'_\nu f'_\mu = \left(f'_{\nu+\mu} + f'_{\nu-\mu}\right)/2$ with the sign included in the definition. Then, the following result is derived:

$$\begin{aligned} &\hat{G}_X\{f_\nu(\boldsymbol{R}')\} \simeq \frac{x_\nu}{k_\nu}\frac{\partial f_\nu}{\partial \Theta_\nu}, \quad \hat{G}_Y\{f_\nu(\boldsymbol{R}')\} \simeq \frac{y_\nu}{k_\nu}\frac{\partial f_\nu}{\partial \Theta_\nu}, \\ &\hat{G}_Z\{f_\nu(\boldsymbol{R}')\} \simeq -\frac{1}{2P}\sum_{\mu=0}^{\infty}\tilde{\zeta}_\mu\left(k_{\nu+\mu}f_{\nu+\mu} + k_{\nu-\mu}f_{\nu-\mu}\right). \end{aligned} \tag{A.4}$$

The operation of $\hat{G}_{X,Y}$ is the derivative with respect to X' or Y'. On the other hand, $\hat{G}_Z$ generates the spectral components with the sum or difference of wavenumbers of the interface profile (μ: profile mode) and the applied magnetic field (ν: magnetic mode), due to the nonlinear mode coupling.

Appendix B. Interface magnetic field in the linear harmonic analysis

We confirm here the interface magnetic field analysis in Section 2 by deriving the interface magnetic field in the linear harmonic analysis when a homogeneous vertical magnetic field is applied on the two-dimensional horizontal interface of magnetic fluid with infinite depth.

By the intensity of the applied magnetic field H_0, basic fields are expressed as

$$h_X^0 = \boldsymbol{t}_X \cdot \boldsymbol{h}^0 = H_0\frac{\partial z^1}{\partial X}, \quad b_Z^0 = \frac{\boldsymbol{t}_Z \cdot \boldsymbol{h}^0}{P} = \frac{H_0}{P},$$

where h_X^0 is small in the linear analysis. In the two-dimensional analysis, $\hat{G}_Y = 0$ as well as $h_Y^0 = 0$. If the interface profile is composed of a unique mode $\mu = m$ changing only in the X-direction, $z^1 = \tilde{\zeta}_m f_m$. Then from (A.4),

$$\begin{aligned} \hat{G}_X\{f_\nu(\boldsymbol{R}')\} &\simeq \frac{1}{k_\nu}\frac{1}{\left|\boldsymbol{r}_X\right|}\frac{\partial f_\nu}{\partial X}, \\ \hat{G}_Z\{f_0(\boldsymbol{R}')\} &\simeq -\frac{1}{P}\frac{\tilde{\zeta}_m}{2}\left(k_{0+m}f_{0+m} + k_{0-m}f_{0-m}\right) \\ &= -\frac{1}{P}k_m\tilde{\zeta}_m f_m = -\frac{1}{P}k_m z^1 f_0, \end{aligned} \tag{B.1}$$

where $\hat{G}_Z$ is supposed to operate on homogeneous fields, and the symmetry $k_{-m} = k_m$, $f_{-m} = f_m$ are used. Accordingly, $\hat{G}_X$ operates as the differentiation with respect to X, and $\hat{G}_Z$ multiplies $-k_m z^1/P$, which causes the variation to the homogeneous magnetic field by the nonlinear mode coupling.

In the linear analysis, $k_m z^1 \ll 1$, and $M\hat{G}_Z$ in (2) is small together with $M/P < 1$. When $\tilde{h}_Z = -Mb_Z^0 = -M_{\rm n}/2$ is supposed to be homogeneous, induced fields are derived from (2), as follows:

$$\begin{aligned} h_X^1 &\simeq \hat{G}_X(1 - M\hat{G}_Z)\tilde{h}_Z = \hat{G}_X(-M\hat{G}_Z\tilde{h}_Z) \\ &\simeq \frac{1}{k_m\,|\boldsymbol{r}_X|}\frac{\partial}{\partial X}\left(\frac{Mk_m z^1}{P}\tilde{h}_Z\right) = -\frac{M}{P}\frac{1}{|\boldsymbol{r}_X|}\frac{\partial z^1}{\partial X}\frac{M_{\rm n}}{2}, \end{aligned} \tag{B.2}$$

$$\begin{aligned} b_Z^1 &\simeq \hat{G}_Z(1 - M\hat{G}_Z)\tilde{h}_Z \simeq \hat{G}_Z\tilde{h}_Z \\ &\simeq -\frac{k_m z^1}{P}\tilde{h}_Z = \frac{k_m z^1}{P}\frac{M_{\rm n}}{2}. \end{aligned} \tag{B.3}$$

The tangential magnetic field h_X^1 is infinitesimal of higher order than h_X^0 by M^2. On the other hand, b_Z^1 is the variation of the normal magnetic flux proportional to the interface elevation z^1, which has been used for the conventional analysis.

References

[1] M. D. Cowley, R. E. Rosensweig, The interfacial stability of a ferromagnetic fluid, J. Fluid. Mech. 30 (4) (1967) 671–688.

[2] R. E. Zelazo, J. R. Melcher, Dynamics and stability of ferrofluids: Surface interactions, J. Fluid. Mech. 39 (1) (1969) 1–24.

[3] A. Gailitis, Formation of the hexagonal pattern on the surface of a ferromagnetic fluid in an applied magnetic field, J. Fluid Mech. 82 (3) (1977) 401–413.

[4] E. Twombly, J. W. Thomas, Mathematical theory of non-linear waves on the surface of a magnetic fluid, IEEE Trans. Magn. MAG 16 (2) (1980) 214–220.

[5] E. E. Twombly, J. W. Thomas, Bifurcating instability of the free surface of a ferrofluid, SIAM J. Math. Anal. 14 (4) (1983) 736–766.

[6] A. G. Boudouvis, J. L. Puchalla, L. E. Scriven, R. E. Rosensweig, Normal field instability and pattern in pools of ferrofluid, J. Magn. Magn. Mater. 65 (1987) 307–310.

[7] Y. Mizuta, Interface magnetic field analysis for free surface phenomena of magnetic fluid, Magnetohydrodynamics 44 (2) (2008) 155–165.

[8] R. E. Rosensweig, Ferrohydrodynamics, Cambridge University Press, Cambridge, 1985, Ch. 7.

Figure Caption

Figure 1: (a) Comparison of the interface stress response h_μ and the induced part of the normal magnetic flux $b_Z^1/\,\tilde{z}_\mu^1$ in the wavenumber space between the linear harmonic analysis (lines) and the numerical analysis (dots) for two-dimensional interface profile under the critical magnetic field intensity $H_{\rm CL}$. (b) Wavenumber distribution of the numerical interface magnetic field h_X, b_Z.

Figure 2: (a) Dependence of the smallest eigenvalue h of H on the intensity of the applied magnetic field H_0 for (1) ζ_0=0.2×10^{-4} [m] (open circle) and (2) ζ_0=5.0×10^{-4} [m] (closed circle). (b) Branch line in the (H_0, ζ_0) plane for two-dimensional interface profile.

Figure 3: (a) Interface profile of hexagonal lattice. (b) Spectral components for interface profile (circles), linear dispersion relation (shaded squares) and critical wavenumber (curve). (c) Branch line in the (H_0, ζ_0) plane for hexagonal-lattice interface profile.

Figure 4: Wavenumber spectra of interface stresses at $h = 0$ for hexagonal-lattice interface profile.

Figure 5: Relative average and standard deviation of the spectra of the interface stresses for hexagonal-lattice interface profile.

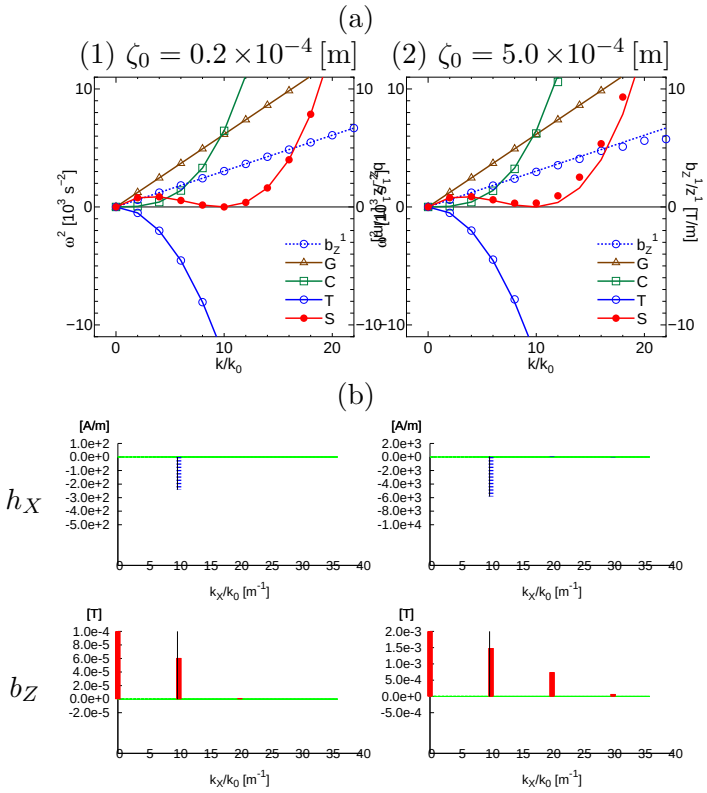

Figure 1:

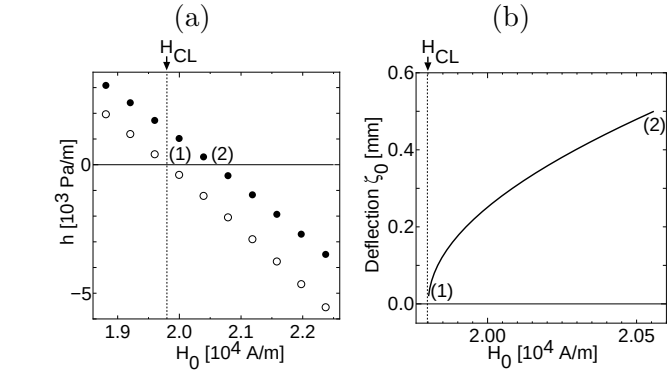

Figure 2:

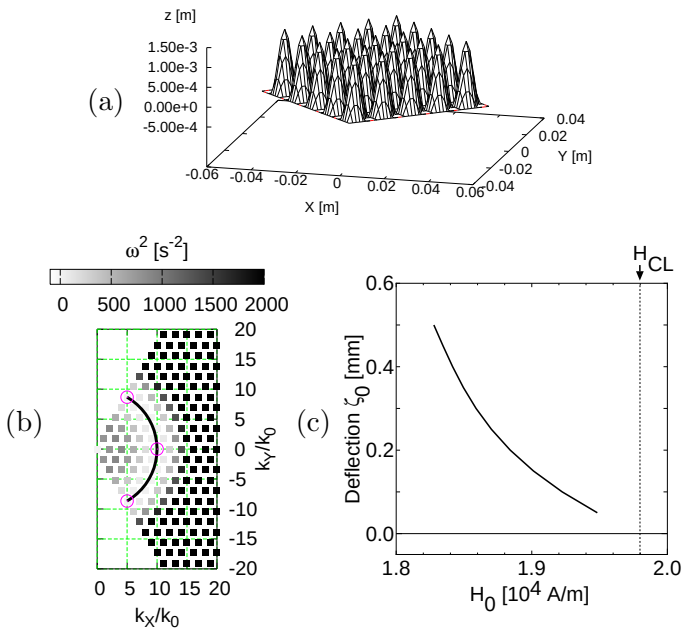

Figure 3:

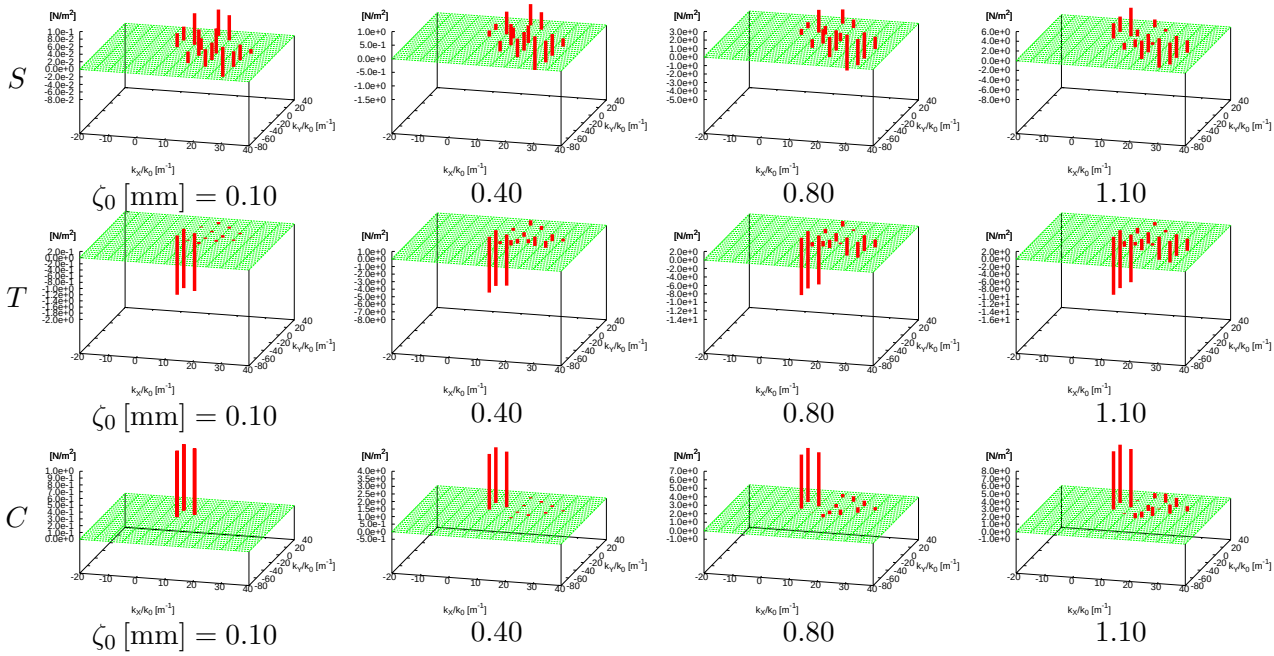

Figure 4:

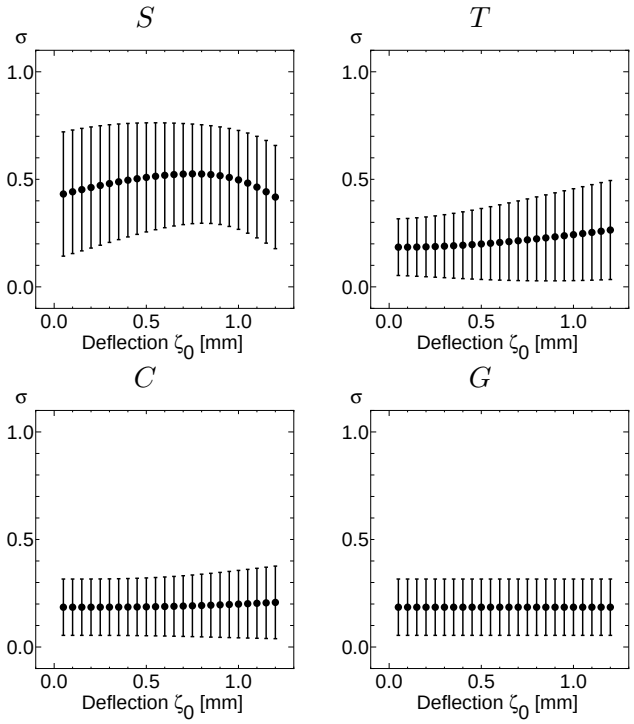

Figure 5: